IEEE Access
Multidisciplinary | Rapid Review | Open Access Journal

Received 8 July 2024, accepted 1 August 2024, date of publication 5 August 2024, date of current version 15 August 2024.

Digital Object Identifier 10.1109/ACCESS.2024.3438837

RESEARCH ARTICLE

Cost-Effective Design of Dual Airgap Permanent Magnet Vernier Machine Having a Yokeless Consequent Pole Rotor

MUDASSIR RAZA SIDDIQI[1,2], MUHAMMAD HUMZA[3], TANVEER YAZDAN[4], AND JIN HUR[1], (Fellow, IEEE)

[1]Electrical Engineering Department, Incheon National University, Incheon 22012, South Korea
[2]Department of Electrical Engineering, KTH Royal Institute of Technology, 10044 Stockholm, Sweden
[3]Department of Electrical, Electronics, and Communication Engineering Education, Chungnam National University, Daejeon 34134, South Korea
[4]Electrical Engineering Department, The University of Lahore, Lahore 54000, Pakistan

Corresponding author: Jin Hur (jinhur@inu.ac.kr)

This work was supported by Incheon National University under the Research Grant 2022-0068.

ABSTRACT In this paper, the cost-effective design of a Dual Airgap Permanent Magnet Vernier Motor (DAPMVM) with a Yokeless Consequent Pole Rotor (YCPR) is presented. The novelty of this research lies in its consequent pole structure of yokeless rotor which is used to maximize the performance attributes while reducing the PM utilization in the dual air-gap PMVM. PMVMs can achieve a high torque density; however, the higher number of poles in the rotor means a higher amount of permanent magnets and hence, a higher cost for the motor. Effective flux modulation and a reduction in eddy current losses are made possible by the YCPR design, which does away with the rotor's yoke. 2D-FEM is used to analyze the performance of the presented model. The simulation results illustrate the potential of the suggested DAPMVM with a YCPR with high torque per magnet volume and reduced losses at rated as well as at higher speeds.

INDEX TERMS Permanent magnet vernier motor, dual airgap, yokeless rotor, consequent pole structure, torque per magnet volume.

I. INTRODUCTION

High torque-density electric motors are gaining special consideration in industries such as robotics, electric vehicles, cranes, and wind power generation, etc. Different types of motors, including PM synchronous motors, double-airgap motors, harmonic motors, and transverse flux motors are being investigated [1], [2]. Direct-drive motors, which do not require mechanical gears, are becoming very popular in high-torque, low-speed applications. These devices may be built with a high power density, good speed, and good operating efficiency since they use high-energy permanent magnets [3], [4], [5], [6], [7]. Nonetheless, large structures with sub-par performance could arise from the mechanical design of motors for direct drive industrial applications. Therefore, the interest in improving the torque density and reducing PM consumption in these motors has increased in the research as well.

Permanent magnet vernier motors have been getting much attention among other direct drive motors due to their high torque density at low-speed operation [8], [9], [10]. PMVMs operate on the basis of the flux modulation effect, also known as the "Magnetic Gearing Effect," which states that a small rotor rotation causes a high flux change in the motor and hence produces high torque [11], [12]. In [13], the initial PMVM model was proposed, and in [14], the design details of PMVM were presented. It was demonstrated in [11] that a vernier motor's flux modulation effect allows it to produce an electromotive force (EMF) of more than two times that of a traditional permanent magnet (PM) motor. Consequently, the high torque density of PMVMs is considered one of their key features. A dual-rotor PMVM is presented in [15], it exhibits a torque density that is almost 50% greater than that of a single-rotor PMVM. In literature, dual-stator vernier motors

The associate editor coordinating the review of this manuscript and approving it for publication was Jorge Esteban Rodas Benítez.

are presented as a way to increase torque density and make use of the space in the single-stator vernier motor. A multipole dual-stator vernier motor was introduced, combining the benefits of two motors in one topology: the inner stator employs the vernier structure, and the outer stator uses the fractional-slot focused winding [16]. Spoke-type PMs were used in dual-stator vernier motors in [17] and [18], and it was demonstrated that this arrangement resulted in a higher torque density and power factor when compared to a single-stator vernier motor. High-temperature superconductor (HTS) bulks have also been used to boost PMVM's torque density [19]. However, using a large number of rotor PM pole pairs is a major disadvantage of PMVMs. The motor's cost is much increased since a large number of PM pole pairs are utilized. A unique dual-stator PMVM was recently proposed in [20], outperforming a traditional single-stator vernier motor in torque density and efficiency. Unfortunately, the presented motor uses PMs on both the inner stator and the rotor, which raises the motor's cost.

In order to reduce leakage flux and increase motor torque density, consequent-pole vernier motors have been proposed in the literature. Reference [21] introduced a consequent-pole vernier motor including toroidal winding. Compared to a standard PMVM, it generates 20% more back EMF while using only 60% of the permanent magnet. A consequent-pole vernier motor with a Halbach array was presented in [22], and it was demonstrated that this motor delivers a torque density that is 55% higher than the reference motor. Moreover, another dual stator PMVM using a consequent pole structure was presented in [23] to increase torque density and reduce the cost of the magnet as compared to the reference motor. The increasing prices of permanent magnets are compelling researchers for cost-effective designs of motors.

This paper presents the design and analysis of an innovative dual airgap PMVM aiming at maximizing the performance compared to the conventional structures. The originality of this research lies in a consequent pole structure of a yokeless rotor. The basic purpose of introducing the consequent pole structure in the dual airgap PMVM is to reduce the usage of PM material while improving the torque density of the motor per unit magnet volume as well as reducing losses. The proposed motor combines the effects of the yokeless rotor in dual airgap PMVM and consequent pole structure to achieve a high torque density per unit magnet volume of the motor.

The paper is comprised of the following sections: Initially, the dual airgap PMVM model's structure, specifications, and working principle with conventional and consequent pole structure will be presented. Moving further, the finite element analysis results of no-load and load analysis of the consequent pole model will be presented and compared with the conventional model. Moreover, the comparison of the conventional and proposed motors will be presented at different speeds. The conclusion of the paper will be presented at the end.

II. PMVM MODEL STRUCTURE, SPECIFICATIONS, AND WORKING PRINCIPLE

Fig. 1(a) and Fig. 1(b) show the structural layout of the dual stator radial flux (DSRF) PMVM with a conventional [26] and proposed consequent pole yokeless rotor, respectively. Table 1 contains the detailed specs of the dual airgap PMVM model with a yokeless rotor. As shown in Fig. 1(a), the model is made up of a sandwiched yokeless rotor and two stators. In order to achieve the flux modulation effect, both stators have traditional toothed pole configurations. Twelve slots and three phases of winding with a four-pole distributed type design are present in the inner and outer stators. The rotor of the motor does not contain any magnetic core, and twenty magnet poles are fixed with the help of a non-magnetic support.

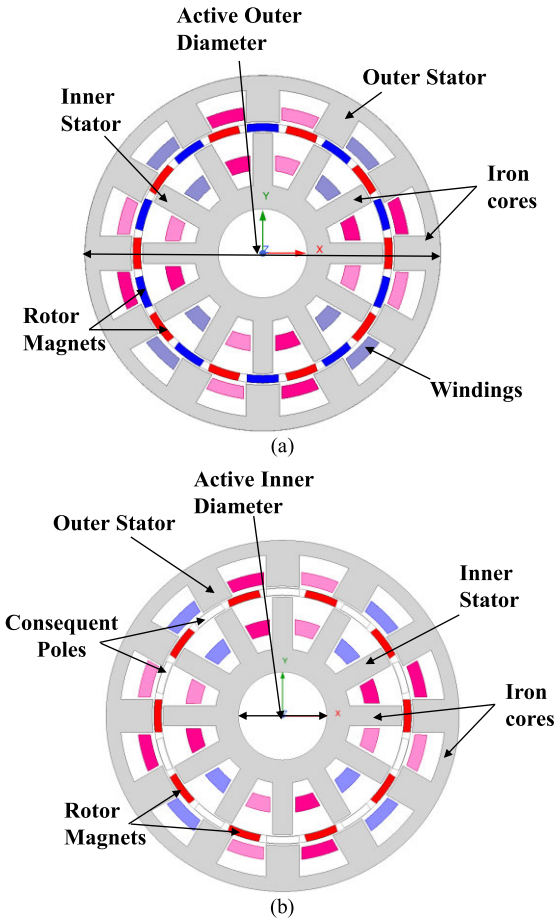

FIGURE 1. The structural layout of the DSRF-PMVM DSW model with the yokeless rotor (a) Conventional (b) Proposed.

The configuration of the proposed model is shown in Fig. 1(b). The model contains two stators and a rotor similar to the existing conventional motor. However, there is a key difference from the conventional motor that instead of the normal PM configuration, consequent pole PMs are used in the yokeless rotor. The presented dual airgap PMVM having a yokeless consequent pole rotor is obtained by redesigning the

TABLE 1. Specifications of the DSRF-PMVM model.

Parameter	Units	Values (Conventional/Proposed)
Active outer diameter of the stator	mm	120
Active inner diameter	mm	30
Outer diameter of the inner stator	mm	81.1
Active axial length	mm	100
Number of rotor pole	-	20
Number of stator slots	-	12
Number of poles of the stator winding	-	4
Length of air gap	mm	0.7
Stator core material	-	S50PN470
Magnet type	-	NdFeb (Br=0.5 T, Hc= -304 kA/m)
Rotor core material	-	Non-magnetic SUS304
Volume of magnet	dm^3	0.053/0.02565
Motor volume	dm^3	1.06
Number of turns per Slot (outer/inner)	-	70/70
Slot fill factor (outer/inner Stator)	%	50/50

rotor of the conventional reference model. The design flow of the consequent pole model is shown in Fig. 2.

This configuration reduces the magnet volume in the proposed motor. The magnet volume in the conventional motor is 0.053 dm^3 as compared to the 0.025 dm^3 magnet volume in the proposed motor. Hence a 53% reduction in the magnet volume is proposed in the consequent pole structure.

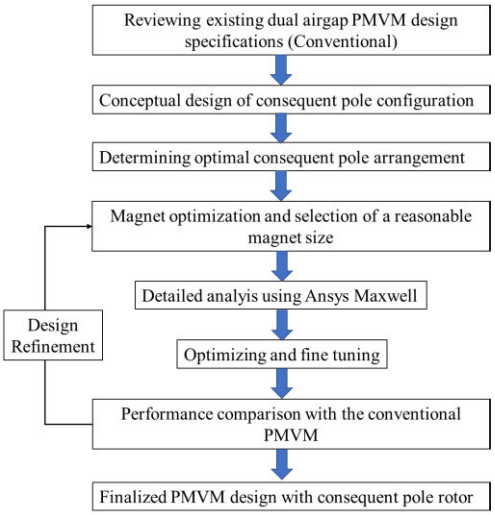

FIGURE 2. Design flow for consequent pole rotor PMVM.

As stated in [24], the PMVMs' working principle is based on the flux modulation effect. The rotor poles provide a high-order harmonic field, whereas the stator windings produce a low-order harmonic field. The torque is produced by modulating these two fields. This phenomenon, known as the ''magnetic gearing effect,'' causes a large flux change with only a tiny rotor spin, producing a large torque. The relationship between the number of stator slots (Z_s), rotor poles (Z_r), and stator winding poles (P_s) is provided by (1) in order to obtain this gearing effect:

$$\pm P_s/2 = Z_r/2 - Z_s \tag{1}$$

The MMF is generated in the airgap with a Z_r number of rotor poles as the rotor rotates. The MMF ($F_{g.m}$) is expressed by (2) [25]:

$$F_{g,m}(\theta, \theta_m) = F_{PM} \sum_{m=odd}^{2} \{1/m * \cos(mZ_r(\theta - \theta_m))\} \tag{2}$$

where θ is the reference axis of rotation, F_{PM} is the airgap MMF's magnitude, θ_m is the rotor position, and m is the harmonic order. The specific airgap permeance of the motor is given by (3):

$$\Lambda(\theta) = \Lambda_0 \sum_{n=1}^{\infty} (\Lambda_n * \cos\theta) \tag{3}$$

where Λ_n is the nth harmonic co-efficient and Λ_0 is the average permeance. The motor's air gap length and slot geometry can be used to determine these coefficients. The airgap flux density is the product of the airgap permeance function and airgap MMF as shown by (4):

$$\begin{aligned} &B_{g.\,m}(\theta, \theta m) \\ &= F_{g.m}(\theta, \theta_m)\,\Lambda(\theta) \\ &= F_{PM}\cos(Z_r(\theta - \theta_m))\{\Lambda_0 - \Lambda_1\cos(Z_s\theta)\} + B_{har} \end{aligned} \tag{4}$$

Λ_1 represents the 1st harmonic of permeance in the formula (4). And B_{har} denotes the higher-order harmonics in the airgap flux density. Instead of writing each harmonic separately, we have collectively defined them as B_{har}. Equation (4) demonstrates that the airgap flux density is the combination of the modulation and the PM magnet flux as shown in Fig. 3. The flux wave similar to the ordinary PM motor is represented by ξ_{m0} whereas the modulated flux resulting from the vernier effect is represented by ξ_{mn}. The same equations can be applied to both air gaps.

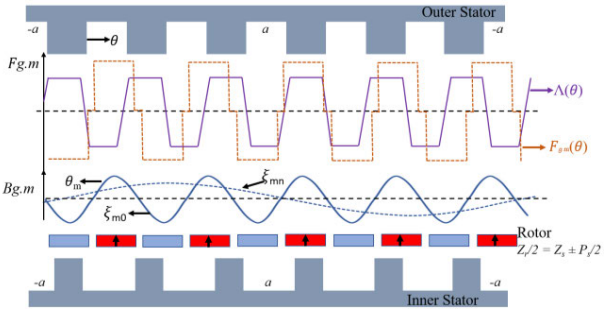

FIGURE 3. Airgap permeance, MMF and Flux density from PM for one airgap.

When a motor has a consequent-pole design, it means that the rotor has only N or S poles. The rotor core, between the permanent magnets, collects magnetic lines of force to generate mixed magnetic poles, which replace some of the original permanent magnets. As the conventional motor has no core due to the yokeless structure of the rotor, we have

placed iron pieces in place of the south pole to complete the consequent pole rotor structure. The flux path of the conventional model is demonstrated in Fig. 4(a). It shows the flux path of the winding poles and the rotor magnetic poles. The flux path appears to start at the rotor's north pole, go through the outer airgap and outer stator, then enter the rotor's south pole and outer airgap before passing through the inner stator to complete the one full winding pole. In this manner, twenty magnet poles are coordinated to form four winding poles. The flux path of the proposed consequent pole model, as shown in Fig. 4(b), follows the same pattern as the conventional dual airgap PMVM model.

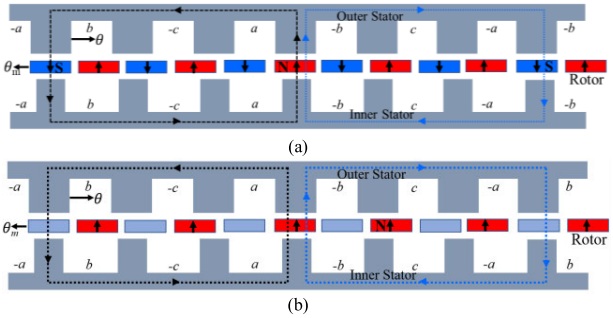

FIGURE 4. Flux path (a) Conventional (b) Proposed.

III. COMPARISON BETWEEN CONVENTIONAL AND PROPOSED MOTOR

In order to analyze the performance of the proposed motor, the 2D transient analysis was performed using the commercial software Ansys Maxwell. Both the conventional and the proposed motor were simulated on similar conditions and the results were compared. All the main design parameters including current density, slot fill factor, motor diameter, winding arrangement, stator and rotor material, and stack length are kept the same for both motors as mentioned in Table 1.

A. RELUCTANCE AND WINDING INDUCTANCE

The reluctance and inductance of the motor play a very important role in the production of useful flux linkage and hence the torque density of the motor. The reluctance of the motor mainly depends upon the circuit geometry and material properties of the circuit components as mentioned in [26]. Fig. 5 shows that the south magnet is absent from the flux path in the case of the proposed model. This means the overall reluctance of the flux path will be reduced in the case of the proposed model as shown in Fig. 5. Here, R_{g1}, R_m, R_{g2}, $\emptyset$ represent the reluctance of the inner airgap, magnet, outer airgap, and flux path respectively. In Fig. 5(b) one R_m is missed in the reluctance circuit due to the absence of one south magnet in the flux path as compared to the reluctance of the conventional model shown in Fig. 5(a).

Fig. 6 shows the comparison between the inductance of the conventional and proposed motor on similar operating

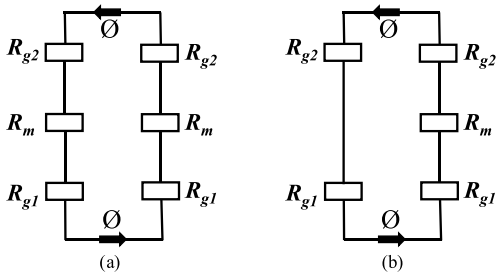

FIGURE 5. Reluctance of flux path (a) Conventional (b) Proposed.

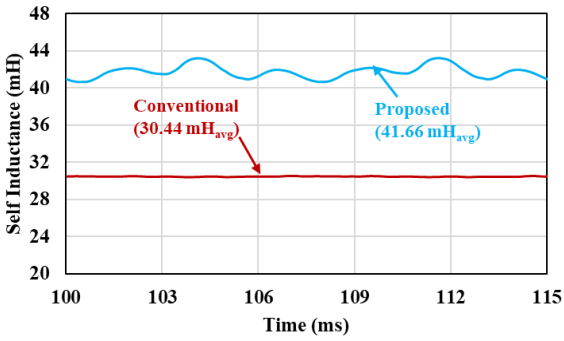

FIGURE 6. Winding inductance comparison.

load conditions. The self-inductance of the proposed motor shows a higher value as compared to the conventional due to reduced reluctance in the proposed motor. The higher inductance in the proposed motor will in turn improve the flux linkage and hence the back EMF of the motor.

B. FLUX LINKAGE, FLUX DENSITY DISTRIBUTION, AND BACK EMF

The flux lines of the conventional motor and the proposed motor at no-load conditions are shown in Fig. 7. The flux in both motors follows the same path shown in Fig. 4.

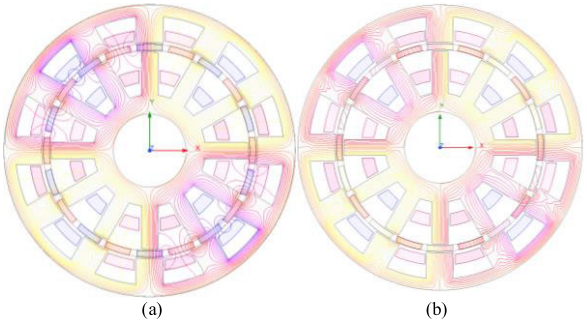

FIGURE 7. Flux lines at no load (a) Conventional (b) Proposed.

The comparison between the flux linkage and flux density of the conventional and proposed motor at no load is presented in Fig. 8 and Fig. 9 respectively. The maximum value of flux linkage in the conventional model is 0.10 Wb, whereas its value is 0.074 Wb in the case of the proposed model. It can be seen that a reduction of only 30% value in flux linkage

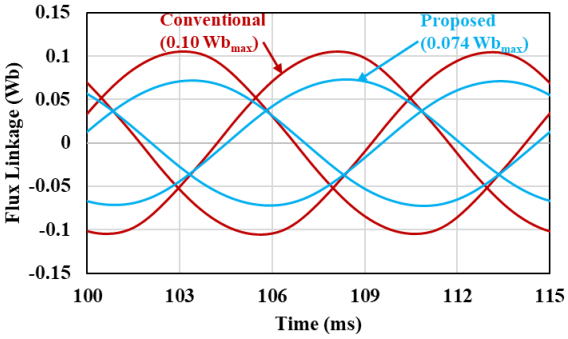

FIGURE 8. Flux linkage comparison.

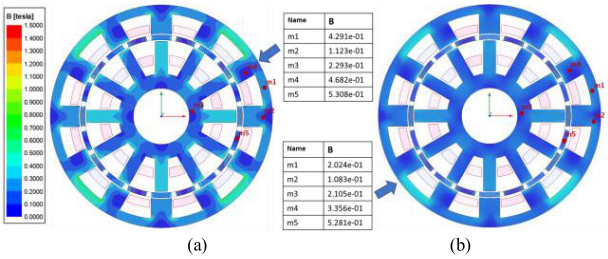

FIGURE 9. Flux density distribution at no load (a) Conventional (b) Proposed.

occurred in the case of the proposed consequent pole structure while the magnets in the proposed model are reduced to 50% as compared to the conventional model. This is due to the higher inductance because of the yokeless rotor between two stators as presented in [26].

The no-load flux density of the conventional and proposed motor is shown in Fig. 9. On a similar scale, the flux density in the conventional model in Fig. 9(a) is higher as compared to the proposed consequent pole model in Fig. 9(b). This is due to the reduced amount of permanent magnets in the proposed model. On the contrary, as shown in Fig. 8, the on-load flux density of the proposed model in Fig. 10(b), is higher than the conventional model in Fig. 10(a), due to an increased winding inductance of the proposed model.

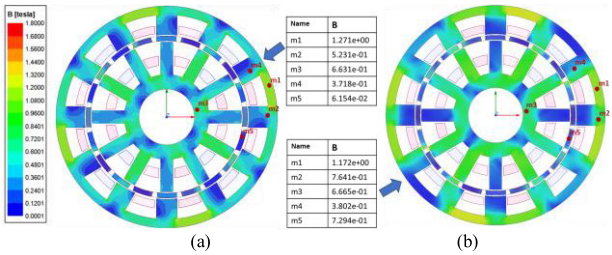

FIGURE 10. Flux density distribution comparison at load (a) Conventional (b) Proposed.

As shown in Fig. 11, the back EMF of the proposed model shows the same trend as flux linkage. The RMS value of the back EMF of the proposed model is 21.43 V which is 70% of the RMS back EMF value (31.08V) of the

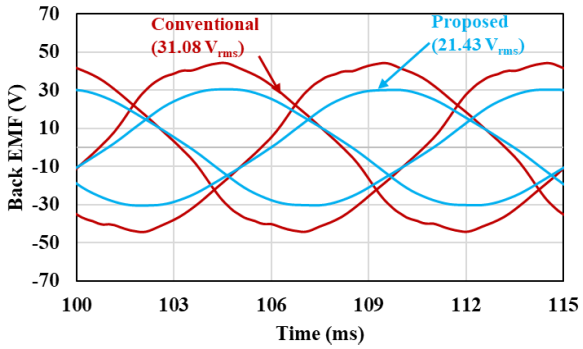

FIGURE 11. Back EMF comparison.

conventional model. Whereas the reduction in magnet size of the proposed consequent pole model is 50% as compared to the conventional model. The FFT results of the back EMF in the conventional model and the proposed model are compared in Fig. 12. It can be seen that the harmonics in both the models have similar frequencies and just the magnitude of the harmonics in the proposed model is reduced due to a reduced back EMF magnitude.

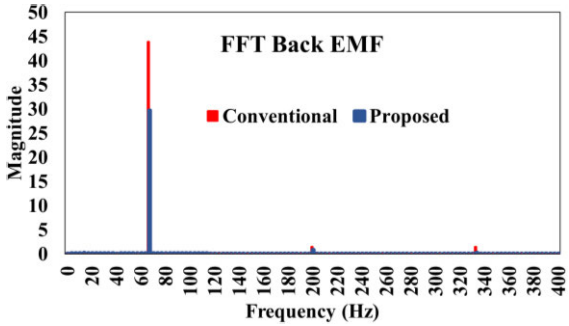

FIGURE 12. Back EMF FFT comparison.

C. OUTPUT TORQUE, TORQUE RIPPLE, AND TORQUE DENSITY

The conventional and proposed models are supplied with same amount of three phase sinusoidal input current to analyze the operation at load conditions. The FFT of the input current is presented in Fig. 13. The frequency of operation of the machine at 400 rpm is 66.7 Hz and the peak value of the input current is 6.7 A as shown in the FFT plot. Moreover, the MMF of each stator is the same in both models. The FFT of the stator MMF is shown in Fig. 14. The significant harmonic is the first one as shown in the graph, whereas the 5^{th}, 7^{th}, $11^{th,}$ and 13^{th} harmonics also exist due to the interaction between slots and the number of poles. The variations in average torque base on pole arc length are shown in Fig. 15. The final dimensions of the consequent pole are decided based on the maximum value of average torque obtained in Fig. 15. The output torque of the conventional motor and the proposed motor at similar rated load conditions is shown in Fig. 16. The average value of torque of the

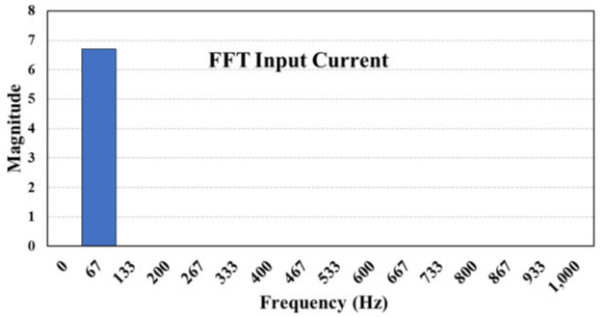

FIGURE 13. FFT of the input three-phase current.

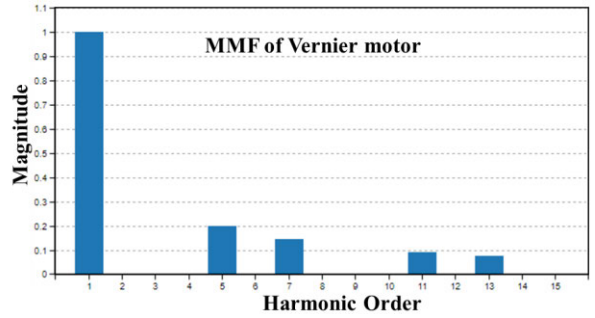

FIGURE 14. FFT of the MMF.

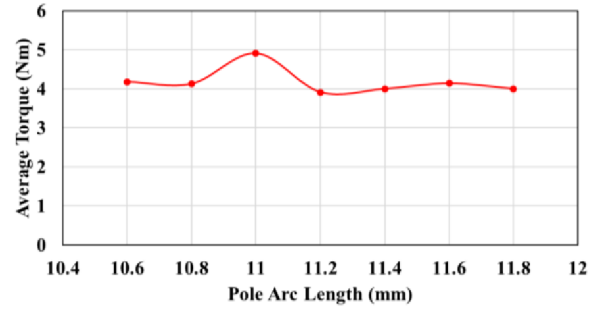

FIGURE 15. Variations in average torque with pole arc length.

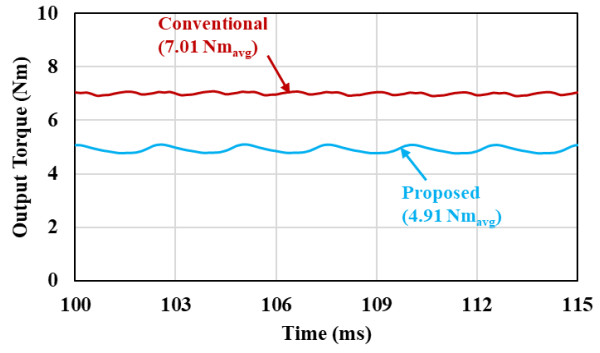

FIGURE 16. Average torque comparison.

conventional motor is higher as compared to the proposed motor. This is due to the higher volume of permanent magnets in the conventional motor. The torque of the proposed motor is 70% of the torque of the conventional motor. Whereas the proposed motor contains 53% less volume of permanent magnets as compared to the conventional motor. Permanent magnets account for a major portion of the total cost of the motor, thus a 53% reduction in the magnet volume means the manufacturing price of the motor will be much reduced.

The torque ripple of the conventional motor is 2.5%, whereas the torque ripple of the proposed motor is 6.7 %. This is a drawback associated with the proposed motor. This is due to the increased reluctance caused by the alternative iron poles on the rotor. The main aim of proposing this model was to reduce the consumption of magnets in the machine and reduce the overall cost of the machine manufacturing. Therefore, the torque ripple increase can be considered a tradeoff for the magnet volume reduction and hence the reduced machine cost.

Furthermore, the torque density per magnet volume of the proposed motor is 196.4 Nm/dm^3 as compared to a value of 132.3 Nm/dm^3 in the conventional motor. This means the torque density per magnet volume of the proposed motor is 47.9% higher than the conventional dual airgap PMVM motor.

D. LOSSES COMPARISON

To compare the efficiency of the conventional and proposed motors, the losses of both motors are calculated and compared based on similar operating conditions. The eddy current loss, hysteresis loss, and core loss of the motors are obtained from the electromagnetic analysis performed with 2D FEM and the results are compared in Fig. 17, Fig. 18, and Fig. 19, respectively.

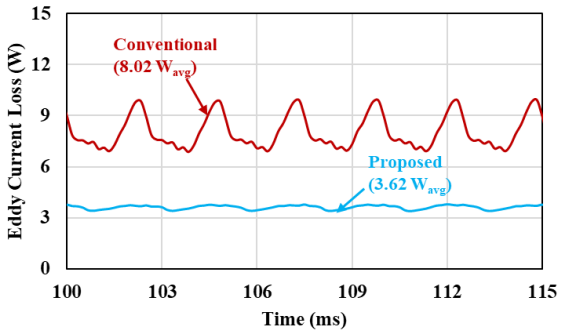

FIGURE 17. Eddy Current Loss comparison.

Fig. 17 shows that the eddy current loss of the proposed motor is reduced as compared to the conventional motor. This is due to the reduced volume of the permanent magnets in the proposed consequent pole motor. The hysteresis loss in Fig. 18 also follows the same trend as the eddy current loss.

As shown in Fig. 19, the average value of core loss of the conventional motor is higher than compared to the proposed motor. Moreover, the two motors have the same stator configurations and the same physical dimensions; the number of winding turns and the input current density in both motors are also the same. Therefore, the copper loss in both motors is also the same. Using 4.7 A_{rms} current and 70 turns in

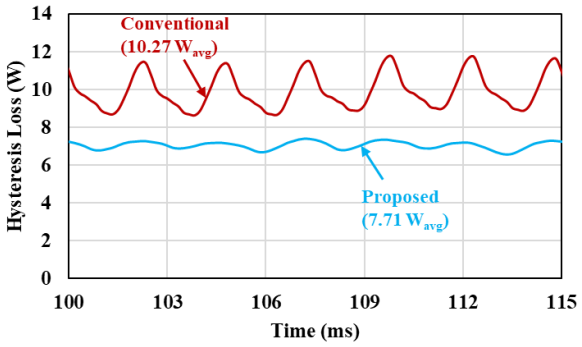

FIGURE 18. Hysteresis Loss comparison.

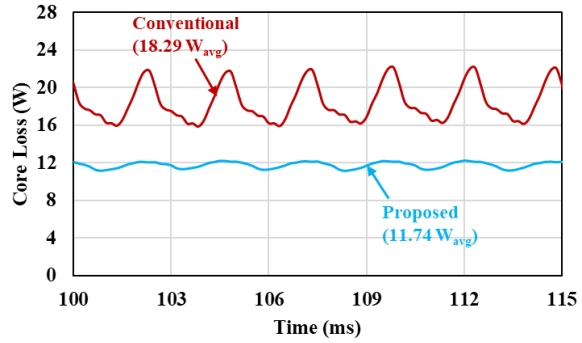

FIGURE 19. Core Loss comparison.

each coil, the copper loss of both motors is calculated to be 34.43 W.

E. EFFICIENCY

The efficiency of the motor is calculated based on the output torque and losses using the following equation (5):

$$\eta = P_{out}\,(P_{out} + P_{losses}) \times 100 \tag{5}$$

The efficiency of the conventional motor is found to be 84 % whereas the efficiency of the proposed motor is 82 %. The slight reduction in efficiency is due to the reduced average torque in the proposed model. Furthermore, the magnet volume used in the proposed motor is 50% less than the conventional motor. The reduction in the permanent magnet cost in the motor is a major advantage of this motor that can be considered a tradeoff to a slight reduction in the efficiency of the motor.

The overall comparison of the DAPMVM with conventional YR and proposed YCPR motors at rated 400 rpm is presented in table 2.

IV. OPERATION AT DIFFERENT SPEEDS

The base speed of the proposed is changed due to the changed inductance in the proposed model. The base speed of the proposed model is calculated to be 304 rpm based on the rotor configuration and inductance. Moreover, the conventional and proposed motors are analyzed at different speeds from 300 to 1000 RPM on similar operating conditions and

TABLE 2. Performance comparison of the conventional and proposed motors.

Parameter	Units	Values	
		Conventional	Proposed
Back EMF	V_{rms}	31.09	21.43
Phase Current	A_{rms}	4.7	
Torque Ripple	%	2.5	6.5
Average Torque	Nm	7.01	4.91
Magnet Volume	dm^3	0.053	0.025
Torque/Magnet Volume	Nm/ dm^3	132,26	196.4
Copper Loss	W	34.43	34.43
Eddy Current Loss	W	8.02	3.6
Hysteresis Loss	W	10.27	7.71
Core Loss	W	18.29	11.31
Efficiency	%	84.0	82.0

the results of the analysis are compared in this section. Fig. 20, 21, and 22 show the comparison between conventional and proposed motors at different speeds based on torque/magnet volume, core loss, and efficiency, respectively.

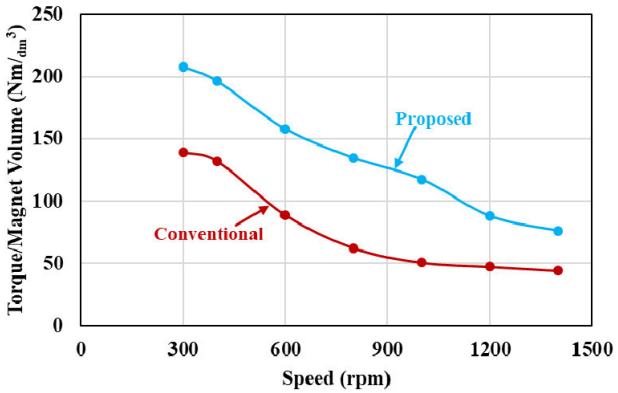

FIGURE 20. Torque/magnet volume comparison.

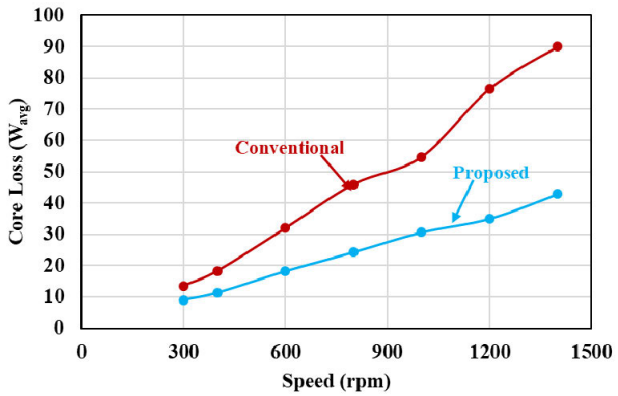

FIGURE 21. Core loss comparison.

As shown in Fig. 20, the torque/magnet volume of the conventional as well as proposed models decreases with an increase in the speed of the motors. However, the overall value of torque/magnet volume is higher in the case of

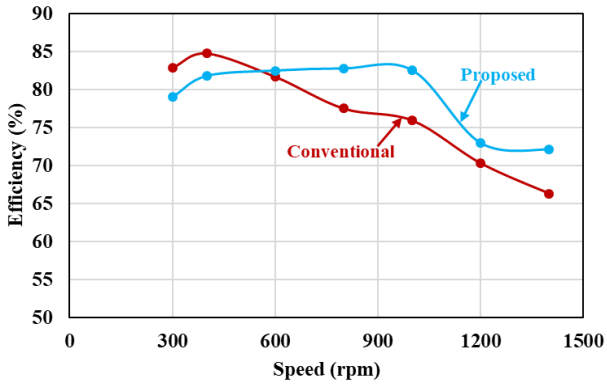

FIGURE 22. Efficiency comparison.

the proposed model as compared to the conventional model throughout the speed range.

Moreover, the core loss of both motors is increased with an increase in the speed of the motor. However, the value of core loss in the case of the proposed model is much less at every speed as compared to the conventional model as shown in Fig. 21.

The efficiency of the proposed motor is lower at low speeds as compared to the conventional motor as shown in Fig. 22. However, the efficiency of the proposed motor is improved at higher speeds as compared to the conventional motor due to much higher losses in the conventional motor at higher speeds.

V. CONCLUSION

In this paper, a special type of Dual Airgap Permanent Magnet Vernier Motor having a yokeless consequent pole rotor (YCPR) is introduced to address the challenge of increased magnet costs due to a higher number of magnet poles in the conventional PMVMs. The implementation of a YCPR provides efficient flux modulation as well as reduces losses in the motor as compared to the conventional motor. Simulation outcomes highlight the potential of the proposed motor, showing a notable increase in the torque per magnet volume while minimizing the utilization of the permanent magnets as compared to the conventional motor on similar operating conditions at rated as well as higher speeds.

REFERENCES

[1] L. Jian, G. Xu, C. C. Mi, K. T. Chau, and C. C. Chan, "Analytical method for magnetic field calculation in a low-speed permanent-magnet harmonic machine," *IEEE Trans. Energy Convers.*, vol. 26, no. 3, pp. 862–870, Sep. 2011.

[2] R. Qu and T. Lipo, "Dual-rotor, radial-flux, toroidally wound, permanent magnet motors," *IEEE Trans. Ind. Appl.*, vol. 39, no. 6, pp. 1665–1673, Dec. 2003.

[3] I. Boldea, Z. Jichun, and S. A. Nasar, "Theoretical characterization of flux reversal motor in low-speed servo drives-the pole-PM configuration," *IEEE Trans. Ind. Appl.*, vol. 38, no. 6, pp. 1549–1557, Nov./Dec. 2002.

[4] Y. Gao, D. Li, R. Qu, X. Fan, J. Li, and H. Ding, "A novel hybrid excitation flux reversal machine for electric vehicle propulsion," *IEEE Trans. Veh. Technol.*, vol. 67, no. 1, pp. 171–182, Jan. 2018.

[5] Y. Du, K. T. Chau, M. Cheng, Y. Fan, W. Zhao, and F. Li, "A linear stator permanent magnet Vernier HTS motor for wave energy conversion," *IEEE Trans. Appl. Supercond.*, vol. 22, no. 3, Jun. 2012, Art. no. 5202505.

[6] J. Li, K. T. Chau, J. Z. Jiang, C. Liu, and W. Li, "A new efficient permanent-magnet Vernier machine for wind power generation," *IEEE Trans. Magn.*, vol. 46, no. 6, pp. 1475–1478, Jun. 2010.

[7] K. Atallah, J. Rens, S. Mezani, and D. Howe, "A novel 'Pseudo' direct-drive brushless permanent magnet machine," *IEEE Trans. Magn.*, vol. 44, no. 11, pp. 4349–4352, Nov. 2008.

[8] D. Li, R. Qu, and T. A. Lipo, "High-power-factor Vernier permanent-magnet machines," *IEEE Trans. Ind. Appl.*, vol. 50, no. 6, pp. 3664–3674, Nov. 2014.

[9] D. Li and R. Qu, "Sinusoidal back EMF of Vernier permanent magnet motors," in *Proc. Int. Conf. Electr. Motors Syst.*, Oct. 2012, pp. 1–6.

[10] S. Ho, S. Niu, and W. Fu, "Design and comparison of Vernier permanent magnet motors," *IEEE Trans. Magn.*, vol. 47, no. 10, pp. 3280–3283, Oct. 2011.

[11] B. Kim and T. A. Lipo, "Operation and design principles of a PM Vernier motor," in *Proc. IEEE Energy Convers. Congr. Exposit.*, Sep. 2013, pp. 5034–5041.

[12] Y. Liu and Z. Q. Zhu, "Magnetic gearing effect in Vernier permanent magnet synchronous machines," in *Proc. IEEE Energy Convers. Congr. Exposit. (ECCE)*, Cincinnati, OH, USA, Oct. 2017, pp. 5025–5032.

[13] A. Ishizaki, "Theory and optimum design of PM Vernier motor," in *Proc. 7th Int. Conf. Electr. Mach. Drives*, Durham, U.K., 1995, pp. 208–212.

[14] S. Niu, S. L. Ho, W. N. Fu, and L. L. Wang, "Quantitative comparison of novel Vernier permanent magnet motors," *IEEE Trans. Magn.*, vol. 46, no. 6, pp. 2032–2035, Jun. 2010.

[15] A. Toba and T. A. Lipo, "Generic torque-maximizing design methodology of surface permanent-magnet Vernier machine," *IEEE Trans. Ind. Appl.*, vol. 36, no. 6, pp. 1539–1546, Dec. 2000.

[16] S. Niu, S. L. Ho, and W. N. Fu, "A novel direct-drive dual-structure permanent magnet machine," *IEEE Trans. Magn.*, vol. 46, no. 6, pp. 2036–2039, Jun. 2010.

[17] B. Kim and T. A. Lipo, "Analysis of a PM Vernier motor with spoke structure," *IEEE Trans. Ind. Appl.*, vol. 52, no. 1, pp. 217–225, Jan. 2016.

[18] F. Zhao, T. A. Lipo, and B.-I. Kwon, "Dual-stator interior permanent magnet Vernier machine having torque density and power factor improvement," *Electric Power Compon. Syst.*, vol. 42, no. 15, pp. 1717–1726, Nov. 2014.

[19] N. Baloch, S. Khaliq, and B. I. Kwon, "A high force density HTS tubular Vernier motor," *IEEE Trans. Magn.*, vol. 53, no. 11, Nov. 2017, Art. no. 8111205.

[20] Y. Gao, R. Qu, D. Li, H. Fang, J. Li, and W. Kong, "A novel dual-stator Vernier permanent magnet motor," *IEEE Trans. Magn.*, vol. 53, no. 11, Nov. 2017, Art. no. 8110105.

[21] D. Li, R. Qu, J. Li, and W. Xu, "Consequent-pole toroidal-winding outer rotor Vernier permanent-magnet motors," *IEEE Trans. Ind. Appl.*, vol. 51, no. 6, pp. 4470–4481, Nov./Dec. 2015.

[22] K. Xie, D. Li, R. Qu, and Y. Gao, "A novel permanent magnet Vernier motor with Halbach array magnets in stator slot opening," *IEEE Trans. Magn.*, vol. 53, no. 6, Jun. 2017, Art. no. 7207005.

[23] N. Baloch, B.-I. Kwon, and Y. Gao, "Low-cost high-torque-density dual-stator consequent-pole permanent magnet Vernier machine," *IEEE Trans. Magn.*, vol. 54, no. 11, pp. 1–5, Nov. 2018, doi: 10.1109/TMAG.2018.2849082.

[24] M. Raza, W. Zhao, T. A. Lipo, and B.-I. Kwon, "Performance comparison of dual airgap and single airgap spoke-type permanent-magnet Vernier machines," *IEEE Trans. Magn.*, vol. 53, no. 6, pp. 1–4, Jun. 2017, doi: 10.1109/TMAG.2017.2669105.

[25] M. Azeem, M. Humza, and B. Kim, "Analytical investigation of air-gap flux density distribution of a PM Vernier motor," *Int. J. Appl. Electromagn. Mech.*, vol. 59, no. 3, pp. 943–949, Mar. 2019.

[26] M. R. Siddiqi, T. Yazdan, J.-H. Im, M. Humza, and J. Hur, "Design and analysis of a dual airgap radial flux permanent magnet Vernier machine with yokeless rotor," *Energies*, vol. 14, no. 8, p. 2311, Apr. 2021.

MUDASSIR RAZA SIDDIQI was born in 1991. He received the bachelor's degree in electrical engineering from the University of Engineering and Technology Taxila, Pakistan, in 2012, the M.S. degree in electrical engineering from the Energy Conversion System Laboratory, Hanyang University, South Korea, in 2017, and the Ph.D. degree from the Department of Electrical Engineering, Incheon National University, South Korea, in 2022. From 2017 to 2018, he was a Researcher with Nex-M Protohouse, Ansan, South Korea. He was a Research Professor of electrical engineering with the Department of Electrical Engineering, Incheon National University, until April 2024. He has been a Postdoctoral Researcher with the Division of Electric Power and Energy Systems, KTH Royal Institute of Technology, Sweden, since May 2024. His research interest includes the design and control of electric motors.

MUHAMMAD HUMZA was born in Jampur, Punjab, Pakistan. He received the bachelor's degree in electrical engineering from FUUAST Islamabad, Pakistan, in 2012, and the M.S. degree leading to the Ph.D. degree in electrical engineering from Kunsan National University, South Korea, in 2018.

He has been an Assistant Professor with the Institute of Southern Punjab Multan, Pakistan. He is currently a Postdoctoral Researcher with Chungnam National University, South Korea. His research interests include electric motors and power electronics.

TANVEER YAZDAN was born in Jampur, Punjab, Pakistan. He received the bachelor's degree in electrical engineering from the University of Engineering and Technology Taxila, Pakistan, in 2010, and the M.S. degree leading to the Ph.D. degree in electrical engineering from Hanyang University, South Korea, in 2018. From 2010 to 2013, he was the Assistant Manager of Karachi-Electric Company, Pakistan. He is currently an Assistant Professor with The University of Lahore, Pakistan. His research interest includes the design and control of electric motors.

JIN HUR (Fellow, IEEE) received the Ph.D. degree in electrical engineering from Hanyang University, Seoul, South Korea, in 1999.

From 1999 to 2000, he was with the Department of Electric Engineering, Texas A&M University, College Station, TX, USA, as a Postdoctoral Research Associate. From 2000 to 2001, he was a Research Professor of electrical engineering for BK21 projects with Hanyang University. From 2002 to 2007, he was the Director of the Intelligent Mechatronics Research Center, Korea Electronics Technology Institute (KETI), South Korea, where he involved on the development of special electric motors and systems. From 2008 to August 2015, he was an Associate Professor with the School of Electric Engineering, University of Ulsan, Ulsan, South Korea. Since August 2015, he has been a Professor with the Department of Electrical Engineering, Incheon National University, Incheon, South Korea. He has authored and co-authored over 140 publications on electric motor design, analysis and control, and power electronics. He has one pending U.S. patent and 20 pending Korean patents. His current research interests include high-performance electrical motors, modeling, drives, new concept actuators for special purposes, and numerical analysis of electromagnetic fields.

Dr. Hur became a fellow of the IEEE Industry Application Society, in 2022. He is an Associate Editor of IEEE TRANSACTIONS ON POWER ELECTRONICS.